



A Conformational Equilibrium in the Nitrogenase MoFe Protein with an α -V70I Amino Acid Substitution Illuminates the Mechanism of H₂ Formation

Journal:	<i>Faraday Discussions</i>
Manuscript ID	FD-ART-11-2022-000153.R1
Article Type:	Paper
Date Submitted by the Author:	06-Jan-2023
Complete List of Authors:	Lukoyanov, Dmitriy A; Northwestern University, Chemistry Yang, Zhiyong; Utah State University, Chemistry and Biochemistry Shisler, Krista; Washington State University, Biological Sciences Peters, John ; University of Oklahoma, Chemistry Raugei, Simone; PNNL, Chemistry Dean, Dennis; Virginia Tech, Department of Biochemistry Seefeldt, Lance; Utah State University, Chemistry and Biochemistry Hoffman, Brian; Northwestern University, Chemistry and Molecular Biosciences

A Conformational Equilibrium in the Nitrogenase MoFe Protein with an α -V70I Amino Acid Substitution Illuminates the Mechanism of H₂ Formation

Dmitriy A. Lukoyanov¹, Zhi-Yong Yang², Krista Shisler³, John W. Peters⁴, Simone Raagei⁵, Dennis R. Dean⁶, Lance C. Seefeldt², and Brian M. Hoffman¹

¹Department of Chemistry and Molecular Biosciences, Northwestern University, Evanston, Illinois 60208, USA.

²Department of Chemistry and Biochemistry, Utah State University, Logan, Utah 84322, USA.

³Institute of Biological Sciences, Washington State University, Pullman, Washington, 99164, USA.

⁴Department of Chemistry and Biochemistry, University of Oklahoma, Norman, Oklahoma, 73019, USA.

⁵Physical and Computational Sciences Directorate, Pacific Northwest National Laboratory, Richland, Washington, 99352, USA.

⁶Biochemistry Department, Virginia Tech, Blacksburg, Virginia, 24061, USA.

Abstract:

Study of α -V70I-substituted nitrogenase MoFe protein identified Fe6 of FeMo-cofactor ($\text{Fe}_7\text{S}_9\text{MoC}$ -homocitrate) as a critical N_2 binding/reduction site. Freeze-trapping this enzyme during Ar turnover captured the key catalytic intermediate in high occupancy, denoted $\text{E}_4(4\text{H})$, which has accumulated $4[\text{e}^-/\text{H}^+]$ as two bridging hydrides, Fe2-H-Fe6 and Fe3-H-Fe7, and protons bound to two sulfurs. $\text{E}_4(4\text{H})$ is poised to bind/reduce N_2 as driven by mechanistically-coupled H_2 reductive-elimination of the hydrides. This process must compete with ongoing hydride protonation (HP), which releases H_2 as the enzyme relaxes to state $\text{E}_2(2\text{H})$, containing $2[\text{e}^-/\text{H}^+]$ as a hydride and sulfur-bound proton; accumulation of $\text{E}_4(4\text{H})$ in α -V70I is enhanced by HP suppression. EPR and ^{95}Mo ENDOR spectroscopies now show that resting-state α -V70I enzyme exists in two conformational states, both in solution and as crystallized, one with wild type (WT)-like FeMo-co and one with perturbed FeMo-co. These reflect two conformations of the Ile residue, as visualized in a reanalysis of the X-ray diffraction data of α -V70I and confirmed by computations. EPR measurements show delivery of $2[\text{e}^-/\text{H}^+]$ to the E_0 state of the WT MoFe protein and to both α -V70I conformations generates $\text{E}_2(2\text{H})$ that contains the Fe3-H-Fe7 bridging hydride; accumulation of another $2[\text{e}^-/\text{H}^+]$ generates $\text{E}_4(4\text{H})$ with Fe2-H-Fe6 as the second hydride. $\text{E}_4(4\text{H})$ in WT enzyme and a minority α -V70I $\text{E}_4(4\text{H})$ conformation as visualized by QM/MM computations relaxes to resting-state through two HP steps that reverse the formation process: HP of Fe2-H-Fe6 followed by slower HP of Fe3-H-Fe7, which leads to transient accumulation of $\text{E}_2(2\text{H})$ containing Fe3-H-Fe7. In the dominant α -V70I $\text{E}_4(4\text{H})$ conformation, HP of Fe2-H-Fe6 is passively suppressed by the positioning of the Ile sidechain; slow HP of Fe3-H-Fe7 occurs first and the resulting $\text{E}_2(2\text{H})$ contains Fe2-H-Fe6. It is this HP suppression in $\text{E}_4(4\text{H})$ that enables α -V70I MoFe to accumulate $\text{E}_4(4\text{H})$ in high occupancy. In addition, HP suppression in α -V70I $\text{E}_4(4\text{H})$ kinetically unmask hydride reductive-elimination without N_2 -binding, a process that is precluded in WT enzyme.

Introduction

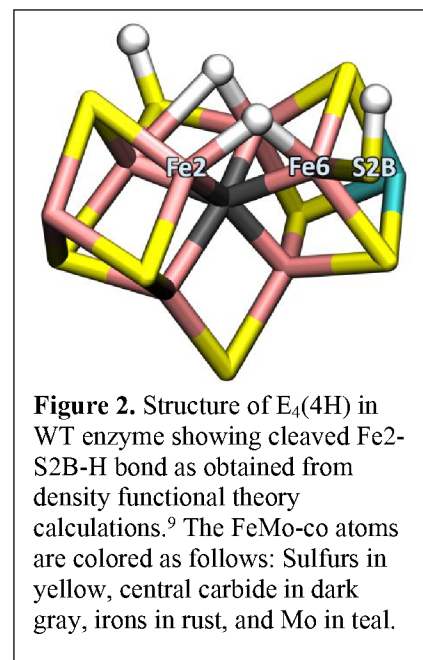
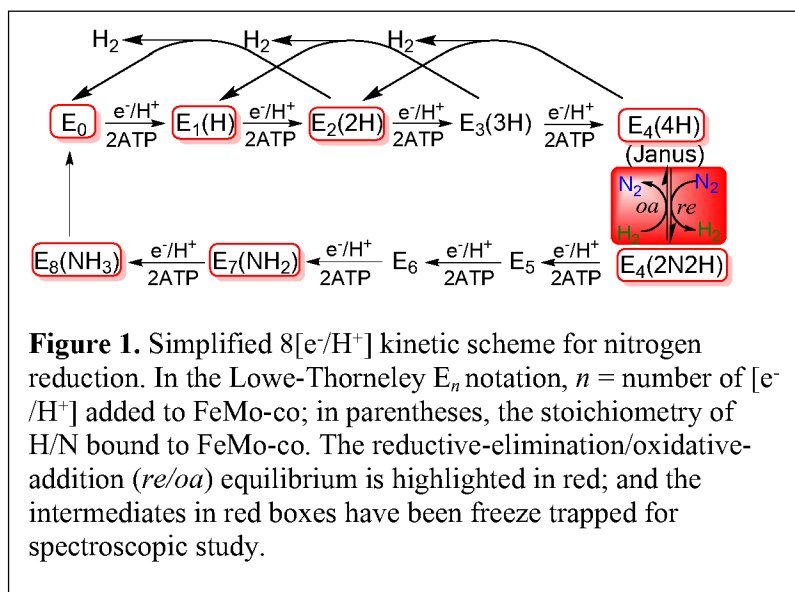
The α -V70I amino acid substituted nitrogenase MoFe protein has played an important role in studies of the mechanism of nitrogen fixation by nitrogenase. A kinetic scheme of this mechanism is summarized in **Fig 1**.¹⁻³ The reported crystal structure of the α -V70I variant revealed that the larger isoleucine sidechain, positioned over Fe6 of the active site FeMo-cofactor, impedes substrate access to this iron, thereby explaining suppression of N₂ reduction in the substituted protein and identifying Fe6 as a critical site on the Fe_{2,3,6,7} face at which N₂ binds.^{4,5} Below we present a more detailed reanalysis of that structure.

Freeze-trapping the α -V70I

MoFe protein during turnover under Ar captures an intermediate in high occupancy that was shown by EPR and ENDOR studies to contain two bridging hydrides, Fe2-H-Fe6 and Fe3-H-Fe7, **Fig 2**.^{6,7} This intermediate also is freeze-trapped in wild type (WT) enzyme, but in low occupancy.⁸ Of particular importance to the present study, the additional protons are bound to the sulfurs that form Fe2-S2B-Fe6 and Fe3-S5A-Fe7 bridges in the resting-state (E₀) structure,⁷ but as will be further discussed below, density function theory (DFT) computations indicated that the Fe2-SH bond in E₄(4H) is hemilabile and can cleave to generate an Fe6-SH moiety, **Fig 2**.⁹

The E₄(4H) state has identical physical properties in the WT and α -V70I MoFe proteins – the same EPR/ENDOR spectra and photolysis characteristics⁸ – but its high occupancy when freeze-trapped in the substituted protein makes it particularly favorable for ENDOR study. However, the WT enzyme importantly also can be freeze-trapped in an N₂-bound state during turnover under N₂.¹⁰ Cryoannealing experiments with WT enzyme freeze-trapped during turnover under N₂, combined with similar experiment with the substituted enzyme freeze-trapped during Ar turnover, showed the N₂-bound state to be E₄(2N2H)¹¹ (**Fig 1**) and established the state with two bridging hydrides to be E₄(4H).¹² This latter is the key state in nitrogen fixation, the Janus intermediate that is activated to bind/reduce N₂ with the concerted reductive elimination of H₂.^{2,8,11}

As a foundation for understanding the behavior of WT enzyme and the α -V70I variant, this report begins by showing that both in solution and as crystallized, the α -V70I variant exhibits two conformational substates. It then examines in detail: (i) what are found to be differing pathways by which WT and α -V70I variant MoFe proteins accumulate [e⁻/H⁺] to form intermediates E₂(2H) and E₄(4H) during Ar turnover, and (ii) the pathways by which these intermediates relax to E₀ by H₂ release through HP.



Materials and Methods.

The *Azotobacter vinelandii* strains DJ 995, DJ1373, and DJ884 expressing the wild-type (WT), α -V70I MoFe protein, and the Fe protein, respectively, were grown and the corresponding proteins were prepared and characterized as previously described.^{6,13} The samples employed to acquire the EPR and ENDOR spectra presented below are specified in **Table S1**.

The α -V70I, ⁹⁵Mo-MoFe protein used for preparation of crystals for EPR measurements was stored in a buffer containing 50 mM Tris, pH 8, 250 mM NaCl, and 2 mM dithionite buffer. Crystals were obtained in about 2 weeks using a micro-capillary batch diffusion method, set up under anaerobic conditions in an MBraun anaerobic chamber, as previously described.^{5,14} The crystals were harvested in an anaerobic Coy chamber, washed with crystallization buffer (diluted with 50 mM Tris, pH 8, 150 mM NaCl to mimic crystallization conditions), and the slurry was loaded into Q-band tubes and quickly frozen in liquid nitrogen.

X-band EPR spectra were measured on an ESP 300 Bruker spectrometer equipped with an Oxford ESR 900 liquid helium flow cryostat. Obtained spectra were simulated with EasySpin software.¹⁵ Q-band CW EPR and pulse ENDOR spectra were acquired at 2 K on spectrometers equipped with liquid helium immersion Dewars as described elsewhere.^{16,17}

Molecular dynamics (MD) simulations were used to refine the X-ray data of the α -V70I variant. Simulations were performed using the protocol described in Ref¹⁸ augmented by umbrella sampling to estimate the relative free energy of potential α -V70I conformations. Quantum chemical calculation based on density functional theory were performed to further refine the structure of the E₀ and E₄(4H) states. These calculations were performed on truncated models of the catalytic pocket as described in Ref.¹⁸ and adopted the BP86 exchange and correlation functional¹⁹⁻²¹ and the def2-TZVP basis set²² for all atoms with the addition of an effective corepotential for Mo.²³

Results and Discussion

α -V70I substitution introduces a MoFe protein conformational equilibrium:

We compared the frozen-solution EPR and ^{95}Mo ENDOR spectra of the WT and α -V70I MoFe proteins in the E_0 resting state, and further compared the EPR spectrum of α -V70I in frozen solution with that in crystals. The EPR spectrum of WT E_0 resting-state frozen solutions exhibits a single $S = 3/2$ signal, named 1a,²⁴ with measured g' -values relative to a fictitious spin $S' = 1/2$ are, $\mathbf{g}' = [4.33, 3.65, 2.01]$, and similarly for single crystals.^{25 26} In contrast, the α -V70I resting state, both in frozen solution and in a frozen polycrystalline slurry, exhibits EPR signals from two conformers of the FeMo-co with different rhombicity. One has an EPR spectrum with essentially the same g' -values as WT enzyme $E_0/1a$, while the other has higher rhombicity, with $g'_1 = 4.53$ (**Fig 3, left**); this perturbed conformation is denoted, $E_0/1a'$. As seen in **Fig 3**, comparable amounts of the two conformers are trapped in frozen solution and in the crystals of the crystalline slurry. However, the relative abundances of the two conformers can vary with sample, which we attribute to the trapping of various non-equilibrium populations.

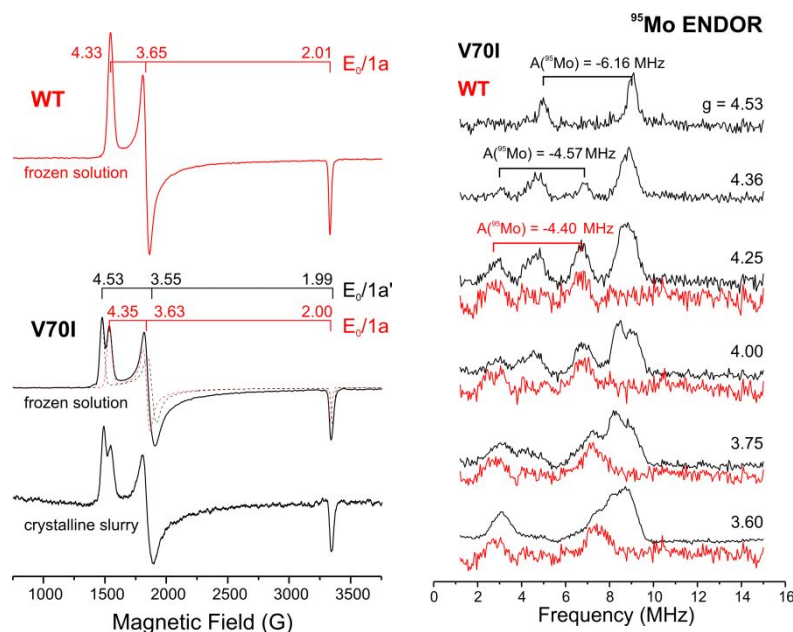


Figure 3. Left, X-band EPR of frozen solutions of WT and α -V70I MoFe proteins in the E_0 resting state, and of a polycrystalline slurry of the latter; dashed lines are EasySpin simulation deconvoluting two conformer of the α -V70I solution resting state. **Right**, Q-band Davies ^{95}Mo ENDOR of the proteins prepared with ^{95}Mo labeling of FeMo-cofactor. Shown ^{95}Mo hyperfine couplings were obtained as described in the text and signed as described in ref 27. **EPR conditions**: temperature, 3.8 K; microwave frequency, ~ 9.36 GHz; microwave power, 0.5 mW; modulation amplitude, 13 G; time constant, 160 ms; field sweep speed, 33 G/s. **ENDOR conditions**: temperature, 2 K; microwave frequency, 34.78 GHz (α -V70I) and 34.72 GHz (WT); Davies sequence, $t(\pi/2) = 40$ ns, $\tau = 600$ ns, RF 40 μs ; repetition time, 5 ms; spectra were taken with noise broaden RF bandwidth and 20 MHz RF filter.

^{95}Mo ($I = 5/2$) Davies ENDOR spectra collected at fields where the EPR spectra of the two conformers overlap show distinct $m_I = \pm 1/2$ doublets from the two conformers (**Fig 3, right**).²⁷ Only one doublet is seen at $g'_1 = 4.53$, where only the higher-rhombicity $E_0/1a'$ signal is present. That doublet is

centered at $A'(\text{obs})/2 = 6.98$ MHz, which corresponds to the hyperfine coupling in the $S = 3/2$ representation of, $A_1 = A'(\text{obs}) \cdot (2/g')$ = 6.16 MHz. This observation of a signal from a single conformer allows assignment of the ENDOR spectra to the appropriate $S = 3/2$ EPR conformer signal where the EPR spectra overlap. At $g'_1 = 4.36$ for the WT conformer, its doublet is centered at $A'(\text{obs})/2 = 4.98$ MHz and corresponds to $A_1 = 4.57$ MHz, essentially the same value previously obtained from ^{95}Mo ENDOR of WT resting state.²⁸ Thus, the influence on FeMo-co of the perturbation associated with the conformation of the large Ile side chain as seen in the E_0 FeMo-co EPR signal, extends to the Mo site of the cofactor.

Crystal structure of α -V70I:

Encouraged by the finding that the α -V70I variant exists in two substates, both in crystals and frozen solution, the structure of the α -V70I variant⁵ was revisited. In this structure the electron density maps of the Ile are ambiguous, and we now find the assignment of two conformations at this position, **Fig 4** refines as well, if not better, than the single conformation previously assigned. MD simulations based on empirical force fields also indicate two conformers, separated by a free energy barrier of 40 kJ/mol, with conformer 1 of **Fig 4** being about 5 kJ/mol more stable in free energy than conformer 2. Refinement of the two conformers using DFT confirms this result. The energy difference from the MD simulations yields relative population of 88% and 12%, but given the uncertainties in relative energies of the two conformers, the computations are compatible with the roughly 1:1 population ratio of the two conformers indicated by both the solution and crystal EPR measurements.

The ethyl arm of the α -Ile70 sidechain approaches S2B more closely in conformer 1 (3.0 Å) than in the other (4.3 Å), **Fig 4**. We propose that this latter conformer corresponds to the perturbed conformer seen spectroscopically, with its g' -shift and ^{95}Mo hyperfine changes for the E_0 conformer of the variant, and that these are caused by the sidechain interactions with FeMo-co, in particular with S2B. We further propose that FeMo-co in the other conformer 2 exhibits properties seen in E_0 of the WT enzyme, which thus represents the unperturbed conformer.

α -V70I conformational interconversion, N_2 reduction and $E_4(4H)$ accumulation

The substitution of the α -V70, which 'sits' over Fe6 of FeMo-co, by isoleucine, with its larger sidechain, causes the specific activity for N_2 reduction to $2NH_3$ to decrease by $\sim 2/3$, with an even greater decrease in specific activity for acetylene reduction.⁴ This effect established that N_2 and C_2H_2 react at Fe6, with the isoleucine sidechain interfering with their access. The observation that the α -V70I variant shows two distinct E_0 conformers modulates the interpretation of its decreased specific activity for N_2 reduction by suggesting that ambient-temperature turnover likewise involves multiple conformers, and that they have different reactivities. As one possible limiting interpretation, $E_4(4H)$ would also exhibit two types of conformers ('two-conformer limit') at ambient temperature, one showing WT reactivity (R conformers), the other with N_2 binding blocked (U conformers). In an opposing limit, at ambient there would be an ensemble of conformational states with a range of degrees of N_2 inhibition. In this case, the crystal-structure and solution results would then imply that this ensemble collapses upon cooling/crystallization into two sub-ensembles/conformers. This issue is addressed below in measurements of the kinetics of loss of E_0 during low-flux Ar turnover of WT and α -V70I MoFe protein.

As shown in the kinetic scheme of **Fig 1**, N_2 binds to $E_4(4H)$ with concerted reductive elimination (*re*) of its two bridging hydrides as H_2 . It is simple to show that if $E_4(4H)$ exhibits the two-conformer limit

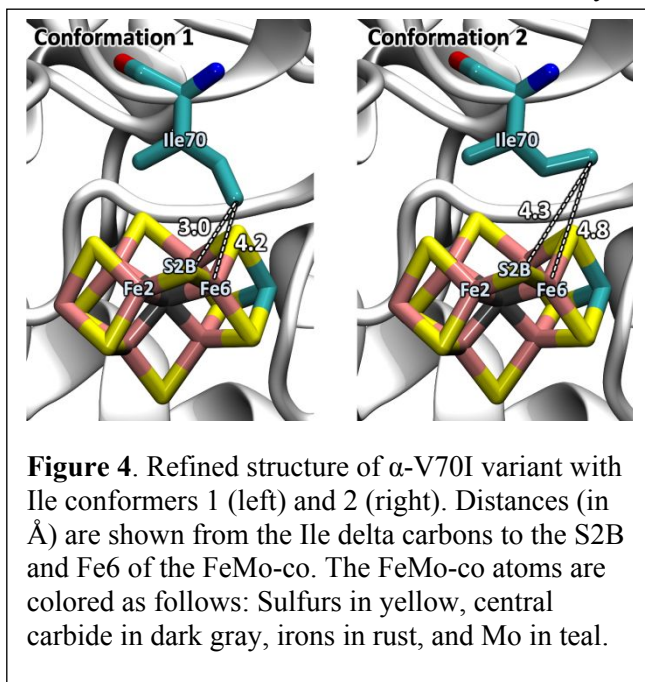


Figure 4. Refined structure of α -V70I variant with Ile conformers 1 (left) and 2 (right). Distances (in Å) are shown from the Ile delta carbons to the S2B and Fe6 of the FeMo-co. The FeMo-co atoms are colored as follows: Sulfurs in yellow, central carbide in dark grey, irons in rust, and Mo in teal.

at ambient temperature, one showing WT reactivity (R conformer), the other being unreactive (U conformer), then the rate constant for N_2 -binding/reductive-elimination would be reduced by $s = 1/(1 + K_c)$, where $K_c = [U]/[R]$ is the equilibrium ratio between interconverting U and R conformers. The measured $s \sim 1/3$ during catalytic N_2 reduction at ambient temperatures then would imply $K_c \sim 2$. These two conformers presumably correspond to the two observed in frozen-solution and crystals of the resting-state enzyme. In the following measurements, we examine conformational contributions to reactivity by examining frozen solutions, and as encouraged by low-flux measurements to be described, discuss them in terms of the two-conformer limit.

Rapid freeze quench and the reaction of reduced Fe-protein with α -V70I conformers: To test the reactivity of the reduced Fe protein with the α -V70I conformers, Fe-protein \rightarrow α -V70I MoFe-protein electron transfer was studied by rapid-freeze-quench (RFQ) techniques, in which solutions of reduced Fe protein (Fe-red) and α -V70I MoFe were rapidly mixed with ATP to initiate electron transfer, then frozen at predetermined times subsequently: 35, 320, and 1600 ms (Fig 5). The early-time sample shows that

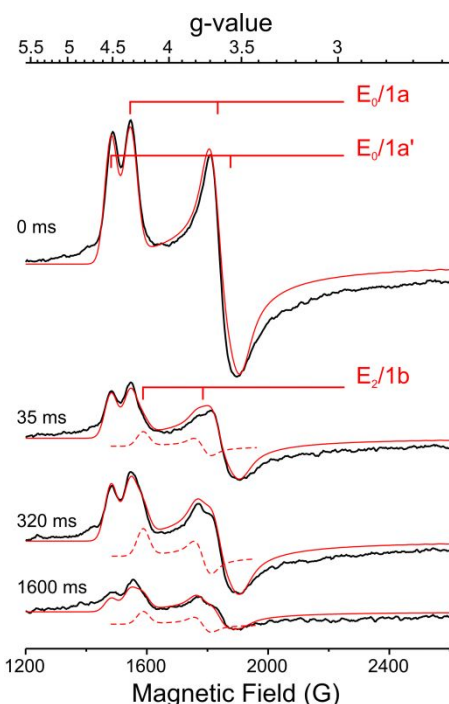
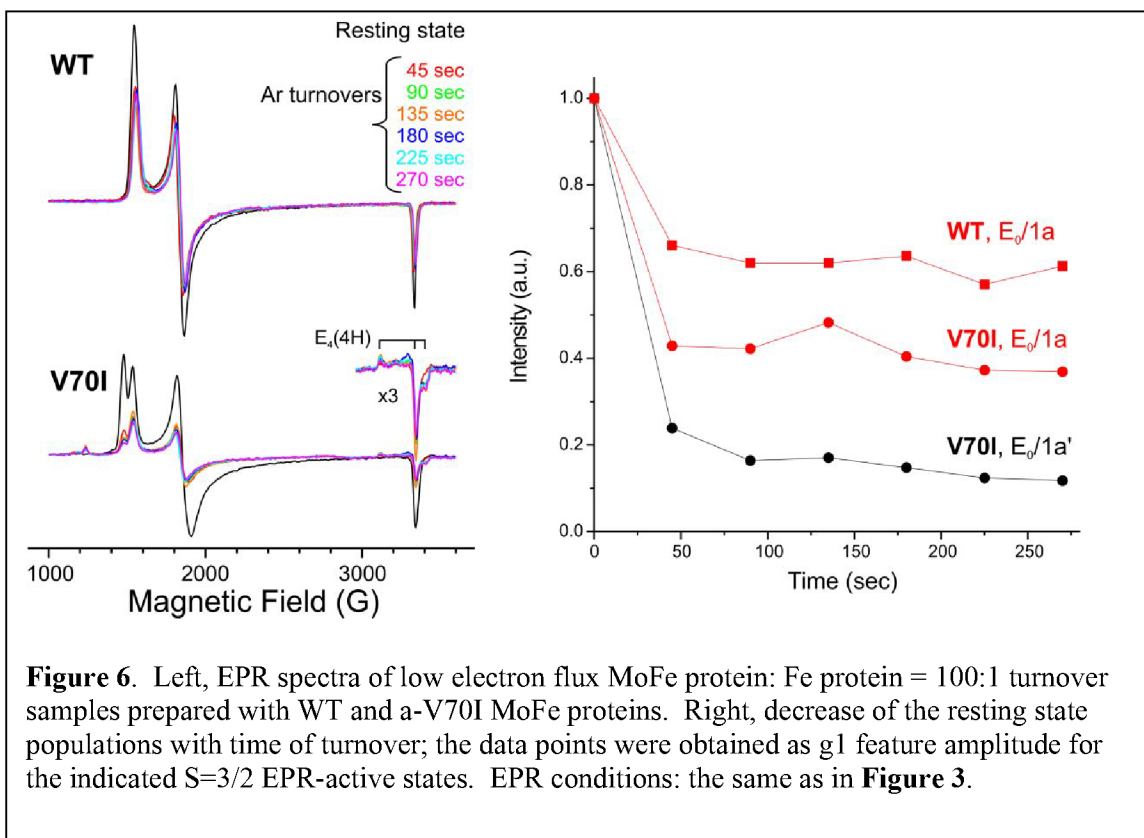


Figure 5. EPR spectra of rapid freeze quenched samples prepared during α -V70I Ar turnover under high electron flux (MoFe protein: Fe protein = 1 : 10). Solid red lines are EasySpin simulations, which are sums of contributions from 1a, 1a', and 1b as discussed in text. Dashed red lines exhibit the contributions of $E_2(2H)/1b$. **EPR conditions:** the same as in Figure 3.

during reduction of E_0 α -V70I MoFe the signals from the two frozen-state conformers decrease in parallel, with roughly 2/3 of each having been reduced by 35 ms while the 1b signal of the $E_2(2H)$ state appears concomitantly. Thus, the two conformers show the same rate of electron accumulation. The $E_2(2H)/1b$ signal increases through 320 ms of reaction and then decreases along with further decrease of the E_0 conformer signals in favor of accumulation of the $E_4(4H)$ state, which appears after 1600 ms (not shown). The $E_4(4H)$ accumulation in α -V70I is much greater than seen for WT enzyme, indicating that this is associated with the presence of the perturbed α -V70I conformer $E_0/1a'$.

Population estimates of the high spin states obtained as described previously²⁹ show that in the RFQ time range of 35 – 320 ms, the combined population of $E_0/1a$ and $E_0/1a'$ states decreases to $\sim 40\%$ and stays unchanged, while population of $E_2(2H)/1b$ accounts for $\sim 20\%$. This distribution is consistent with populations of $E_0/1a$ and $E_2(2H)/1b$ previously observed in similar RFQ experiment for WT enzyme,³⁰ and is roughly in accordance with prediction of the Lowe and Thorneley kinetic model.³¹ Considering that none of the other $E_2(2H)$ signals discussed below are seen in spectra of RFQ samples, it can be concluded that *both α -V70I conformers - $E_0/1a$ and $E_0/1a'$ - form only $E_2(2H)/1b$ upon two-fold reduction.*

Low-flux turnover of WT and α -V70I; implication for conformational equilibrium and rates of HP at ambient temperatures: Given the above observation that the electron-accumulation is unaffected by the α -V70I substitutions, the observation of enhanced $E_4(4H)$ populations with α -V70I implies that the amino acid substitution decreases the HP rate constant of the perturbed α -V70I conformation. In confirmation of this conclusion, such a decrease also is observed in turnover measurements at ambient temperatures under extremely low electron flux, which is achieved by mixing MoFe and Fe proteins in very unequal proportion of 100 MoFe per 1 Fe protein.^{29,32} After several minutes of such low-flux turnover of the WT enzyme approximately half the cofactors of the WT enzyme are reduced, **Fig 6**, yet EPR spectra show no noticeable traces of $E_2(2H)/1b$ (or $E_4(4H)$), indicating that the ‘missing’ E_0 resting state has been reduced to the EPR-silent state $E_1(H)$. In short, the WT nitrogenase had reached a steady-state equilibrium involving only the two states, E_0 , $E_1(H)$. This arises because under this low-flux condition, electron delivery to cofactor in WT enzyme is too slow to compete with HP at the $E_2(2H)$ state. Once a second electron/proton is delivered to $E_1(H)$ to form $E_2(2H)$, H_2 generation by HP and its release outcompetes electron delivery to achieve more-reduced states. Remarkably, this behavior is exactly as predicted by the kinetic scheme of **Fig 1** for low-flux steady state turnover: no matter how small the flux, if steady state is achieved, then states E_0 and E_1 are predicted to have equal populations, 50% of the total.



The low-flux behavior of the α -V70I variant is dramatically different. As shown in **Fig 6**, freeze-trapping α -V70I during low-flux turnover shows that its unperturbed resting state $E_0/1a$ conformer undergoes the same ~ 50 - 60% loss as for WT upon reaching steady state, but the perturbed conformer $E_0/1a'$ shows an $\sim 90\%$ resting-state loss, accompanied by the appearance of reduced E-states, even including the dihydride $E_4(4H)$. In consonance with cryoannealing observations presented below, this shows that the rate constant for HP relaxation of $E_2(2H)$ for the perturbed conformer is so small that even under such low-flux condition, further reduction of this conformer outcompetes HP in $E_2(2H)$, and causes near-complete depopulation of the E_0 conformer in favor of the accumulation of states that have received two and more electrons. In particular, the intensities of $E_4(4H)$ signals for WT enzyme are much less than

those for α -V70I when freeze-trapped during Ar turnover under the modestly low electron flux ($[\text{Fe}]/[\text{MoFe}] \sim 1$) that previously was used in order to achieve MoFe protein concentrations high enough for EPR and ENDOR study.⁸ This shows that it is HP-suppression in $E_4(4\text{H})$ of the α -V70I perturbed conformation that leads to freeze-trapping of $E_4(4\text{H})$ in much higher occupancy ($\sim 50\%$ or greater) than for WT enzyme.

With such suppression of HP in α -V70I, it can be inferred (i) that electron-delivery to the HP-inhibited conformation controls its accumulation of $E_4(4\text{H})$, (ii) that the occupancy of the $E_4(4\text{H})$ state in the α -V70I protein freeze-quenched under Ar turnover is a rather faithful measure of the occupancy of the HP-inhibited conformation at ambient temperatures, and (iii) that the interconversion between the conformers is slow, in keeping with the large activation energy calculated for interconversion. In principle, of course a conformational equilibrium will in general be temperature dependent, but this process is not altering the present measurements. Thus, electron delivery from the Fe protein to MoFe protein is relatively slow at ambient temperature, slows with cooling, and it is completely quenched on freezing the aqueous buffer solutions, which occurs not far below 0 °C. Therefore, during the rapid quench-freezing of an aqueous-buffer enzyme solution in dry-ice/acetone or liquid nitrogen, it would be impossible to deliver enough electrons to MoFe to significantly increase the $E_4(4\text{H})$ occupancy as measured, and thus alter the inferred occupancies, while cooling would further slow interconversion.

$E_2(2\text{H})$ states accumulated in turnover and during cryoannealing

Numerous intermediates have been freeze-trapped during turnover of WT and α -V70I MoFe proteins, and cryoannealing measurements have been instrumental in determining the E_n -state they represent.^{11,12,29} This subsection first describes the formation of E_n states $n = 2, 4$, for WT and α -V70I MoFe and phenomena observed during their cryoannealing, then analyzes their cryoannealing kinetics.

WT enzyme: When the electron flux is increased by decreasing the MoFe/Fe ratio from the extreme 100/1 value, but the flux nonetheless remains low enough to keep the highly-reduced WT states $E_3(3\text{H})$ and $E_4(4\text{H})$ essentially depopulated, the most populated EPR-active intermediate trapped by freeze-quench of WT enzyme during turnover under Ar is the $S = 3/2$ state with EPR signal of low rhombicity ($g_1 = 4.21$, $g_2 = 3.76$), known as 1b.²⁴ The identification of the 1b signal with $E_2(2\text{H})$ had been made through the observation that during cryoannealing this signal directly converts into the E_0 resting state signal 1a in a single step, with KIE ~ 3 associated with the protonation of a hydride bound to the cofactor of $E_2(2\text{H})/1\text{b}$ with concomitant release of H_2 .²⁹

There is another $S = 3/2$ conformer of the $E_2(2\text{H})$ state, with EPR signal of higher rhombicity, $g' = [4.69, \sim 3.20, \sim 2]$ and historically named 1c.²⁴ In freeze-trapped WT turnover samples the 1c signal usually is even of lower amplitude than 1b, and is not easy to study. However its assignment to $E_2(2\text{H})$ was first indicated by the observation that 1c decays in a single step during cryoannealing, with relaxation characteristics similar to those of the $E_2(2\text{H})/1\text{b}$ relaxation.²⁹ The definitive assignment of 1c to an $E_2(2\text{H})$ state was achieved through photolysis experiments, which interconvert 1b and 1c, confirming that both signals arise from $E_2(2\text{H})$ conformers.³³

Turnover of WT MoFe under substrate N_2 allows freeze-trapping of $E_4(2N_2H)$, the product of N_2 binding/reduction coupled to H_2 reductive elimination, **Fig 1**. The identification of this state was established by cryoannealing, during which it relaxes in three steps. It oxidatively adds H_2 and loses N_2 , converting to $E_4(4H)$, which in turn converts in a single kinetic step with H_2 loss to the $E_2(2H)/1b$ state. This state decays more slowly than it is formed during cryoannealing, so it first accumulates (1b signal increases) before it in turn decays and converts to $E_0/1a$ with H_2 formation.⁸

α -V70I Enzyme: The α -V70I variant was only studied under Ar turnover because its specific reactivity with N_2 is much lower than WT. Under these conditions, freeze-trapping the α -V70I variant captures large populations of $E_4(4H)$; no $E_2(2H)$ state is trapped. As previously reported,¹² and as shown in **Fig 7**,¹² cryoannealing relaxation of α -V70I $E_4(4H)$ also proceeds to E_0 in two steps, as with WT. However, during annealing, the α -V70I $E_4(4H)$ state does not first relax to $E_2(2H)/1b$. Instead it relaxes to a 'high-rhombicity (hr)' $S = 3/2$ state,¹² denoted $E_2(2H)/hr$, whose EPR signal has rhombicity ($g'_1 = 5.26$, $g'_2 = 2.58$) much greater than that of either the WT $E_2(2H)/1b$ or $1c$ signals. As discussed below, this difference in the $E_2(2H)$ state is ascribable to the presence of different isomers of the $E_2(2H)$ hydride. Relaxation of α -V70I $E_4(4H)$ through the $E_2(2H)/hr$ intermediate primarily generates the mutation-perturbed $E_0/1a'$ resting state conformer. It is important to emphasize that this observation thus confirms that the high populations of $E_4(4H)$ that accumulate during α -V70I turnover are associated with this perturbed conformer.

Cryoannealing relaxation schemes

In this subsection, we develop the schemes for the cryoannealing/relaxation of $E_4(4H)$ and $E_2(2H)$ (**Fig 1**) of WT enzyme freeze-trapped during turnover under N_2 , and of WT and α -V70I MoFe freeze-trapped during turnover under Ar.

For the WT enzyme trapped during turnover under N_2 , the cryoannealing process starts with the trapped diazene-level state $E_4(2N_2H)$ formed by the coupled binding of N_2 and reductive elimination of H_2 from the dihydride $E_4(4H)$ during turnover (**Fig 1**). During cryoannealing at -50 °C, $E_4(2N_2H)$ relaxes to the resting state E_0 in three steps,⁸ the first being oxidative addition of H_2 and release of N_2 to regenerate the $E_4(4H)$ state. As

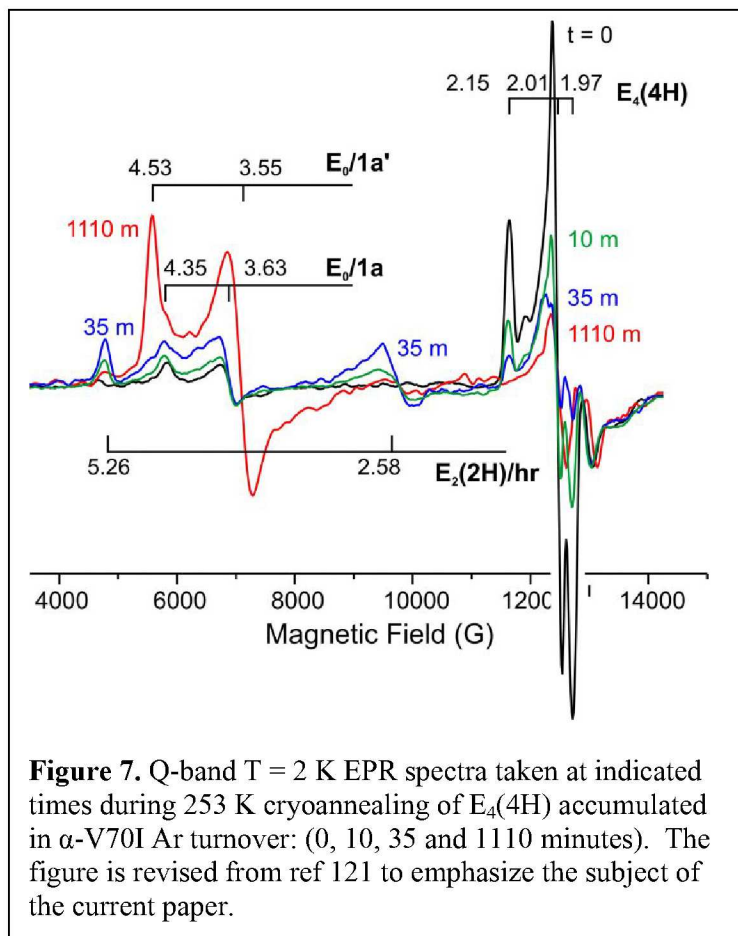
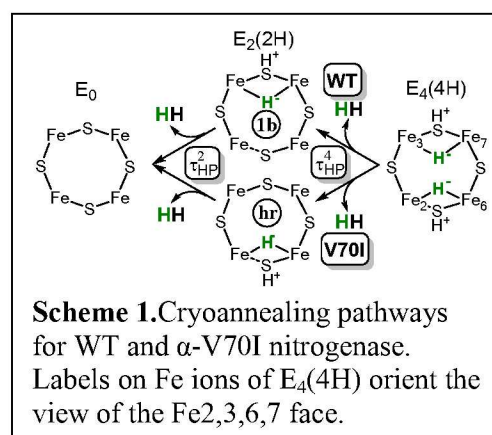


Figure 7. Q-band $T = 2$ K EPR spectra taken at indicated times during 253 K cryoannealing of $E_4(4H)$ accumulated in α -V70I Ar turnover: (0, 10, 35 and 1110 minutes). The figure is revised from ref 121 to emphasize the subject of the current paper.



visualized in **Scheme 1**, WT $E_4(4H)$ then converts to $E_2(2H)/1b$, which in turn relaxes to E_0 , with time constants listed in **Table 1**. Of particular note, the $-50\text{ }^\circ\text{C}$ cryoannealing process for WT enzyme exhibits a sharp, ~ 60 -fold difference in the time constants for HP in $E_4(4H)$ ($\tau_{HP}^4 \sim 6\text{ m}$) and in $E_2(2H)$ ($\tau_{HP}^2 \sim 330\text{ m}$). It is this sharply slower relaxation of $E_2(2H)/1b$ compared to its formation that causes its buildup with subsequent slower decay during cryoannealing. The time constant for relaxation of WT $E_2(2H)/1b$ to E_0 at $-20\text{ }^\circ\text{C}$ also was measured, and found to be 30 times faster, **Table 1**.^{8,12}

Table 1	Cryoannealing/Relaxation Time-constants			
	-50°C		-20°C	
Variant	WT^c	V70I	WT	V70I^d
τ_{HP}^4 ^(a)	6	≥ 600 ^f	-	13
τ_{HP}^2 ^(b)	330		~ 10 ^e	870

(a) Estimates from stretched-exponential fits; (b) exponential fit; (c) *ref 8*; (d) *ref 12*; (e) unpublished; (f) estimated (see text). Note: arrows indicate HP time-constants assigned to Fe3-H-Fe7 (see text)

The α -V70I $E_4(4H)$ likewise relaxes to E_0 in a two-step process that exhibits the buildup then decay of $E_2(2H)$, both steps exhibiting a KIE associated with HP and H_2 release.¹² However, although as noted above, the properties of the $E_4(4H)$ state in α -V70I are identical to those for WT MoFe, in perhaps the most dramatic consequence of the α -V70I substitution, cryoannealing α -V70I $E_4(4H)$ does not produce the $E_2(2H)/1b$ state formed during relaxation of WT $E_4(4H)$, but instead forms the high-rhombicity state $E_2(2H)/hr$, which accumulates then relaxes to E_0 , **Scheme 1**.

The cryoannealing kinetics of the α -V70I variant also show a second remarkable consequence of the substitution: as anticipated above from the buildup of $E_4(4H)$ during turnover, both steps of $E_4(4H)$ relaxation through HP are dramatically slower than in the WT enzyme. Thus, during cryoannealing of α -V70I $E_4(4H)$ at $-50\text{ }^\circ\text{C}$, the temperature used for WT, relaxation was so slow that it was impracticable to carry out this process. Instead, to monitor the annealing process for α -V70I it was necessary to speed up the process by increasing the annealing temperature from $-50\text{ }^\circ\text{C}$ to $-20\text{ }^\circ\text{C}$, and even at this more-elevated temperature the time constants for both annealing steps of α -V70I are more than twice as large as for WT at $-20\text{ }^\circ\text{C}$ (**Table 1**). It should be noted that before choosing $-20\text{ }^\circ\text{C}$ for α -V70I, lower temperatures were tested. With short 5 min annealing steps, no significant loss of the $E_4(4H)$ signal intensity was observed for $T \leq -30\text{ }^\circ\text{C}$, meaning that at each temperature, the time constant for $E_4(4H) \rightarrow E_2(2H)$ conversion during cryoannealing of α -V70I must be extremely large compared to that for WT. To put this in context, assuming we could not have detected a decrease in intensity of $E_4(4H)$ beyond reproducibility error in EPR recording (less than 5%) for 5 min at $-50\text{ }^\circ\text{C}$, then the decay-time of $E_4(4H)$ in α -V70I at this temperature must be at least 100-fold greater than that for WT.

It thus *appears* that the two time constants for relaxation steps of $E_4(4H)$ in α -V70I are increased by comparable factors of ca 100-fold compared to those for WT, accidentally keeping the ~ 60 fold difference between the time constants for the two steps observed for WT. However, as a foreshadowing that the situation will below prove to be more complex, the time-constant for the second relaxation step in WT enzyme at $-20\text{ }^\circ\text{C}$, namely $\tau_{HP}^2(\text{WT})$, for the $E_2(2H)/1b \rightarrow E_0$ relaxation, is essentially the same as that for the first hydride protonation in α -V70I at $-20\text{ }^\circ\text{C}$, $\tau_{HP}^4(\alpha\text{-V70I})$ for the relaxation, $E_4(4H) \rightarrow E_2(2H)/hr$, and this is likewise true for relaxation at $-50\text{ }^\circ\text{C}$ (*See Table 1*). These observations will be shown below to be arise because the influence of the α -V70I substitution is to dramatically slow the HP of the Fe2-H-Fe6 hydride, strongly increasing its time-constant for HP at a given temperature without significant influence on the Fe3-H-Fe7 hydride, **Table 1**. Such an effect would cause the WT and α -V70I variant to follow the alternative cryoannealing pathways as shown in **Scheme 1**, with the first step in the relaxation of $E_4(4H)$ involving a different hydride in the two variants, Fe2-H-Fe6 in WT but Fe3-H-Fe7 in α -V70I, and therefore with different products – $E_2(2H)/1b$ in WT, but $E_2(2H)/hr$ in α -V70I.

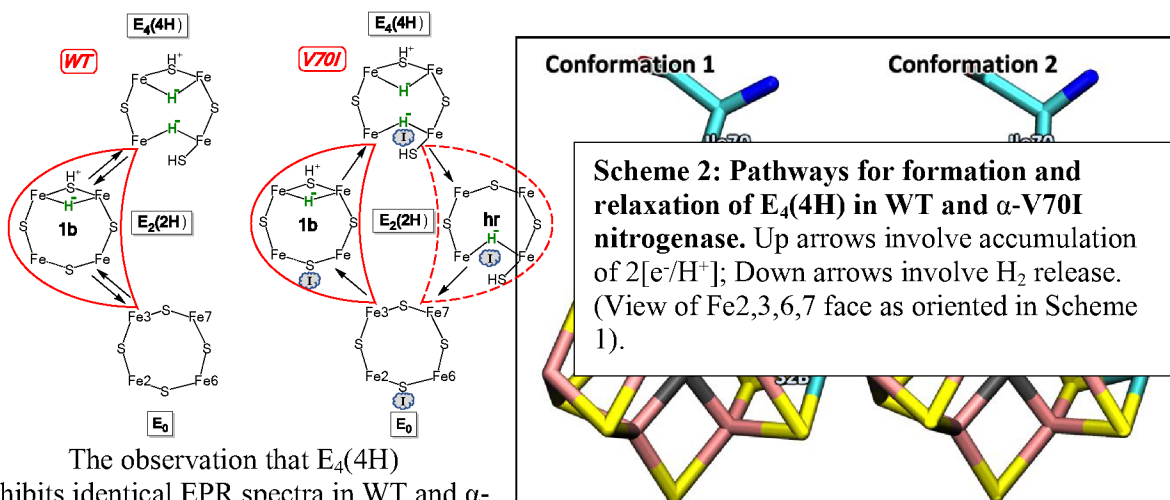
Implications of HP suppression for kinetic studies:

As discussed above, N_2 reduction in α -V70I protein is diminished in comparison with that in WT enzyme because the large Ile sidechain blocks access of N_2 to Fe6, showing that to be the N_2 binding site, and not molybdenum. Trapping a high population of the $E_4(4H)$ dihydride intermediate during turnover of α -V70I, which enabled its detailed ENDOR study, was not expected, and came as a nice bonus. The cryoannealing results presented here demonstrate that accumulation of the $E_4(4H)$ intermediate under Ar turnover of the substituted protein is enhanced because the substitution suppresses protonation of the Fe2-H-Fe6 hydride of $E_4(4H)$, while in doing so the substitution has altered the $E_2(2H)$ state of the protein formed by HP of $E_4(4H)$. As a consequence of this, the enhanced accumulation of $E_4(4H)$ seen in the α -V70I enzyme relative to WT is only partially due to suppression of reaction with N_2 , with a major contribution from suppressed HP at $E_4(4H)$.

The cryoannealing and the ambient-temperature, low-flux measurements (**Fig 6**) agree in showing that the HP rate constants are sharply lower in the α -V70I than in WT enzyme, an indication that the cryoannealing data is a faithful representation of the behavior at ambient. This in turn implies that the direct observation of an ~ 60 -fold difference between rates for HP in $E_4(4H)$ and in $E_2(2H)$, as seen in cryoannealing of both WT enzyme and α -V70I, likewise provides a faithful representation of the behavior at ambient. This conclusion represents a significant modification to the early conclusion based on analysis of previous pre-steady-state kinetic studies, that the HP rates for $E_4(4H)$ and $E_2(2H)$ of WT enzyme differ by less than a factor of two.¹

Structural interpretation of HP suppression in MoFe α -V70I

The formation of different $E_2(2H)$ states during cryoannealing $E_4(4H)$ of WT (1b) and of α -V70I (hi-rhomb/hr), as well as the increased HP time constants seen during α -V70I cryoannealing, can be explained jointly by two assumptions. *First*, that one of the two hydrides of $E_4(4H)$, which we will argue to be the Fe2-H-Fe6 hydride bridge in WT enzyme is intrinsically more reactive to HP than the other hydride, and therefore during relaxation of WT $E_4(4H)$, the Fe2-H-Fe6 selectively undergoes the initial HP reaction to release H_2 and form the $E_2(2H)/1b$ state containing the Fe3-H-Fe7 hydride, as shown in **Schemes 1, 2**. *Second*, the α -V70I substitution selectively inhibits the protonation of the Fe2-H-Fe6 hydride, to the extent that the highly accumulated $E_4(4H)$ in the α -V70I enzyme first releases H_2 through the slow HP of the essentially unperturbed Fe3-H-Fe7 hydride of $E_4(4H)$, forming $E_2(2H)/hr$, which thus we conclude contains the Fe2-H-Fe6 hydride that has become stabilized to HP.



The observation that $E_4(4H)$ exhibits identical EPR spectra in WT and α -V70I enzymes indicates that reduction of N_2 and other substrates in the α -V70I MoFe variant is suppressed because this variant

Figure 8. Structure of $E_4(4H)$ in the α -V70I variant with Ile conformers 1 (left) and 2 (right) at the Ile position as obtained from density functional theory calculations. The FeMo-co atoms are colored as follows: Sulfurs in yellow, central carbide in dark gray, irons in rust, and Mo in teal.

exhibits conformation(s) that *passively* block substrate access to the site of reaction, Fe6, rather than actively altering the reactivity of Fe6. The original report of the α -V70I structure, analyzed in terms of a single Ile conformation, further considered two possible explanations for the increase in the time-constant for HP in $E_4(4H)$ that causes the efficient trapping of $E_4(4H)$ during Ar turnover of this variant.⁵ Both explanations involve mutation-induced suppression of proton delivery to FeMo-co. One postulates the methyl group of isoleucine blocks protonation of the Fe2-H-Fe6 hydride by an H^+ from α -H195. In the other, the enlarged residue blocks H^+ flow from waters adjacent to R-homocitrate. However, the $E_4(4H)$ intermediate has two bridging hydrides, with each having an adjacent sulfur-bound protons available to protonate the hydride. Thus, additional proton delivery to the $E_4(4H)$ form of FeMo-co from the active-site surroundings is unnecessary for HP.

Instead, QM computations now performed with the α -V70I substitution strongly support a third explanation for how this modification enhances accumulation of $E_4(4H)$. As visualized above in **Fig 2**, our previous computations^{9,34} showed the bond between Fe2 and protonated S2B is hemilabile, and the Fe2-S2B bond breaks to create a terminal Fe6-S2B-H sulfhydryl, which ‘swings away’ from its position in E_0 (**Fig 8**).³⁵⁻³⁶ QM refinement of $E_4(4H)$ in α -V70I now indicates that Ile70 can adopt two conformations (**Fig 8**), as observed for E_0 (**Fig 4**), with conformation 1 of $E_4(4H)$ favored over conformation 2 by 25 kJ/mol rather than only 5 kJ/mol as in E_0 .

Firstly, with the H-S2B sulfhydryl of $E_4(4H)$ ‘swung out’, the Ile sidechain of the dominant conformation 1 would not interact with it, in contrast to the interaction with bridging S2B in E_0 , offering an explanation for the absence of substitution-induced changes in the properties of $E_4(4H)$, which are seen for E_0 . *Secondly, and of perhaps greater importance*, this offers the explanation for the substitution-induced change in $E_4(4H)$ HP reactivity. The HP process for $E_4(4H)$ FeMo-co containing the Fe-S2B-H fragment must involve rotation of the S2B-H back towards Fe2, to bring the H^+ on sulfur into contact with the Fe2-H-Fe6 hydride, and computations by Thorhallson and Bjornsson indicate the same situation occurs for HP of this hydride in the $E_2(2H)$ state.³⁷ However, given the conformational flexibility of the Ile side chain proximate to Fe6 in the crystal of resting-state α -V70I, **Fig 4**, we propose that in $E_4(4H)$ the sidechain adopts a conformation that is a variant of conformation 1 of **Fig 4**, in which its $C_{\delta 1}$ methyl group sterically, but passively, blocks the repositioning of the S2B-H sulfhydryl (transient re-formation of the Fe6-S2B bond) that precedes protonation of Fe2-H-Fe6 by the S2B proton. This passive blocking, illustrated in **Scheme 2**, can be viewed as analogous to the sidechain’s passive blocking of the approach of N_2 to Fe6, and would not create substitution-induced changes in the properties of $E_4(4H)$.

We propose it is this steric obstruction that causes the time-constant for HP of hydride Fe2-H-Fe6 during cryoannealing to increase dramatically from its value in WT enzyme, becoming roughly 60-fold longer than for HP of the Fe3-H-Fe7 hydride, and leading to a lengthening of the time-constant for HP of Fe2-H-Fe6 by 3-4 orders of magnitude. Such a decrease in reactivity would make this conformation effectively unreactive to HP, thereby enabling the buildup of $E_4(4H)$ seen with freeze-quench.

This analysis in turn implies that the first step in cryoannealing $E_4(4H)$ trapped in the HP-suppressed conformation of the α -V70I variant, denoted $E_4(4H)_i$, is protonolysis of the Fe3-H-Fe7 hydride, with a time constant largely unchanged by the substitution from that of the second HP of WT, **Scheme 2, Table 1**. This creates the $E_2(2H)$ /hr conformer that retains the Fe2-H-Fe6 hydride, *not* $E_2(2H)$ /1b as forms by relaxation in WT enzyme. The Fe2-H-Fe6 hydride eventually undergoes its sterically-hindered, slow HP with release of H_2 , probably enabled by repositioning of the Ile sidechain, returning the enzyme to the E_0 state.

This proposal not only identifies hydride Fe2-H-Fe6 as undergoing the first hydride protonation of WT $E_4(4H)$, **Scheme 2**; it further identifies the $E_2(2H)$ /1b state, which is both trapped during turnover and produced by cryoannealing/relaxation of WT $E_4(4H)$, as containing the bridging Fe3-H-Fe7 hydride. In short this proposal for the behavior of the α -V70I variant implies that electron/proton

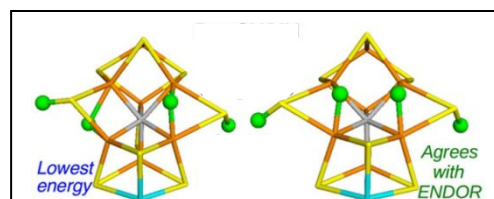


Figure 9. Best QM/MM structures of $E_4(4H)$ have two bridging hydrides, from report by, and with figure adapted from, ref 36. Fe atoms are colored rust, S atoms yellow, H atoms green, Mo atom teal, and C atom gray. The calculated lowest energy state is shown on the left and the proposed structure from ENDOR on the right.

accumulation by WT nitrogenase proceeds through initial formation of $E_2(2H)/1b$, with a Fe3-H-Fe7 hydride bridge. Hydride fluxionality at ambient temperatures could well lead to a dynamic partial hydride transfer to Fe2/Fe6 in $E_2(2H)$, but the trapping of the 1b signal both during turnover and during cryoannealing/relaxation of $E_4(4H)$ indicates that $E_2(2H)/1b$, which has the Fe3-H-Fe7 hydride bridge, is the preferred form. Subsequent accumulation of two additional $[e^-/H^+]$ then leads to formation of $E_4(4H)$

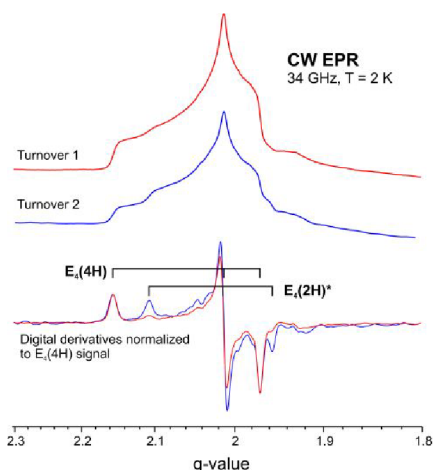


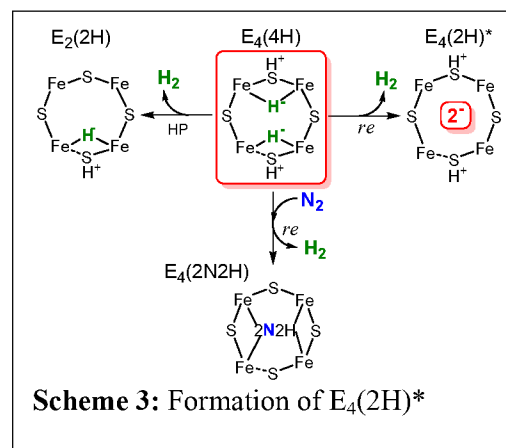
Figure 10. CW, absorption-display rapid passage EPR spectra of two states of the same α -V70I D_2O sample trapped during turnover. ‘Turnover 1’, as trapped; ‘Turnover 2’, which shows increased population of $E_4(2H)^*$, was prepared after complete annealing at $-20^\circ C$ (1110 min), followed by turnover for 15 seconds at $+30^\circ C$. The digital derivatives of the spectra (low) were normalized to $E_4(4H)$ signal amplitude for assignment of the state raised in the ‘Turnover 2’. **EPR conditions:** temperature, 2 K; microwave frequency, ~ 35 GHz; microwave power, 0.32 mW; modulation amplitude, 4 G; time constant, 128 ms; 4 minutes field scans.

with hydrides bridging both Fe3/Fe7 and Fe2/Fe6.

Obstruction by the $C_{\delta 1}$ methyl group of the Ile substituent likewise explains hindered HP in α -V70I if one instead favors either of the two lowest-energy $E_4(4H)$ structures of Cao and Ryde.³⁸ In both of these the Fe2-S2B-Fe6 bridge remains intact, and the two bridging hydrides are each flanked by a bridging SH (Fig 9). However, in their state with parallel bridging hydrides, the adjacent S-H proton is directed ‘away’ from the hydride. The SH group thus must still ‘reorganize’ to bring the nascent H^+ in contact with the hydride, and again the Ile $C_{\delta 1}$ methyl could sterically hinder the reorganization. These considerations however do provide an argument against their alternative, slightly more-stable structure, in which the $C_{\delta 1}$ methyl group would not be likely to hinder protonation (Fig 9). Finally, if one considers the extreme possibility that S2B is actually released from FeMo-co in $E_4(4H)$,³⁶ passive hindrance to its return could explain suppression of HP by the Ile sidechain.

Formation of $E_4(2H)^*$ during Ar turnover of α -V70I protein: An unexpected consequence of the α -V70I substitution is the appearance of an EPR signal whose g-values, $g = [2.11, 2.01, 1.96]$, Figure 10, are characteristic of the state denoted $E_4(2H)^*$.³⁹ The signal is always minor and its intensity varies with preparation of the freeze quenched α -V70I turnover sample. As an example, Fig 10 compares spectra from two turnover samples that clearly show the features of the $E_4(2H)^*$ signal. The SI presents evidence confirming that the signal represents $E_4(2H)^*$ accumulated in low occupancy during turnover of α -V70I.

Formation of $E_4(2H)^*$ state would occur upon the direct reductive elimination of H_2 from $E_4(4H)$ uncoupled from N_2 binding, leaving the two remaining electrons accumulated by $E_4(4H)$ as having doubly-reduced the FeS core of FeMo-co, with the two associated protons bound to sulfur, Scheme S1.^{34,39,40} Previously, the $E_4(2H)^*$ state was only seen upon photolysis of WT $E_4(4H)$;⁸ it is never observed during WT turnover under any atmosphere, neither Ar or N_2 . In particular, this state from $E_4(4H)$ does not play any role in WT turnover under N_2 , as explained directly below.



Why would $E_4(2H)^*$ form during Ar turnover of α -V70I, but not WT turnover? As indicated in **Scheme 3**, direct hydride reductive elimination from $E_4(4H)$ to form $E_4(2H)^*$ must occur in kinetic competition with hydride protonation. The observation that α -V70I under Ar turnover exhibits even a low level of *re* from $E_4(4H)_I$ to form $E_4(2H)^*$ (**Fig 10**) thus implies that in the WT enzyme this process is kinetically outcompeted by the far more rapid hydride protonation of $E_4(4H)$. In short, it appears that in the HP-suppressed α -V70I conformation that accumulates a high population of $E_4(4H)$ the time constant for HP is increased to such an extent that $E_4(2H)^*$ can accumulate to very low, but observable levels.

Summary

The present measurements show that the α -V70I substitution creates two types of active-site conformations in the resting-state (E_0) enzyme, as visualized by reanalysis of the α -V70I crystal structure and QM/MM computations, **Fig 4**. The measurements as supported by computations further suggest accumulation of $E_4(4H)$ is enhanced in α -V70I because this state exhibits sidechain conformation(s) in which steric hindrance by the isoleucine $C_{\delta 1}$ passively blocks protonation of the Fe2-H-Fe6 hydride by the proton on S2B (**Scheme 2**). Prior DFT computations of $E_4(4H)$ indicate that the Fe2-S2B bond in this state is hemilabile and breaks to form an Fe6-S2B-H sulfhydryl that ‘swings away’ from the cofactor (**Fig 2**), while the current QM/MM computations of the $E_4(4H)$ state identify a dominant Ile conformer, **Fig 8**, in which we propose that the Ile $C_{\delta 1}$ blocks the ‘swing-back’ of the Fe6-S2B-H and Fe2-S2B rebinding necessary to bring the sulfhydryl proton and hydride in proximity for HP as visualized in **Scheme 2**. As an alternative possibility, based on computations of Cao and Ryde, $C_{\delta 1}$ blocks repositioning of the proton on an intact Fe2-SH-Fe6 moiety, **Fig 9**. As a result of the steric interference inferred for either model, the time-constant for spontaneous protonation of the Fe2-H-Fe6 hydride, as measured during $E_4(4H)$ cryoannealing, is increased by 3-4 orders of magnitude, thereby changing the order in which the two hydrides are protonated on the 2-step cryoannealing relaxation pathway to E_0 (**Scheme 2**).

As further visualized in **Scheme 2**, both WT and α -V70I variant accumulate four electrons to form the $E_4(4H)$ Janus intermediate (**Fig 1**) through a pathway that leads through the doubly-reduced $E_2(2H)/1b$ intermediate, which stores its two accumulated electrons as an Fe3-H-Fe7 hydride bridge, then proceeds to form $E_4(4H)$, with two hydride bridges, Fe3-H-Fe7 and Fe2-H-Fe6. During relaxation of $E_4(4H)$ in WT enzyme, HP of Fe2-H-Fe6 forms $E_2(2H)/1b$, which contains Fe3-H-Fe7; in $E_4(4H)$ of α -V70I, HP of Fe3-H-Fe7 forms $E_2(2H)/hr$, which contains Fe2-H-Fe6, **Scheme 2**.

The suppression of HP in the $E_4(4H)$ state of α -V70I by *passive* sidechain obstruction, as schematized in **Scheme 2**, is then responsible for the ability to freeze-trap a high population of this state unperturbed by the substitution, with the resulting EPR/ENDOR/photolysis characterization of this state that has played a central role in current understanding of the nitrogenase catalytic mechanism. In addition, it now appears that by strongly slowing HP at the E_4 stage, the α -V70I substitution slightly unmasks a third reaction channel for the $E_4(4H)$ Janus intermediate that is entirely precluded by rapid HP during turnover of WT enzyme: the first-order reductive elimination of H_2 *without* N_2 binding/reduction, to form $E_4(2H)^*$ (**Scheme 3**).

Author Contributions

All authors contributed to the investigation: DRD for genetics and strain construction, ZYY for protein purification and sample preparation, DAL for collection of all spectra, DAL and BMH for spectra interpretation, KS and JWP for X-ray crystallography, SR for calculations. BMH, DAL, and LCS wrote the original draft. All authors contributed to review and editing.

Conflicts of Interest

There are no conflicts to declare.

Acknowledgements

Spectroscopy work was supported by the U.S. National Science Foundation (MCB-1908587, B.M.H.). Clone construction, sample preparation, and X-ray structure determination was supported by the U.S.

Department of Energy (DOE), Office of Science, Office of Basic Energy Sciences (DE-SC0010687, DE-SC0010834, DE-SC0018143 to L.C.S., D.R.D., J.W.P.). S.R. did calculations with support provided by the U.S. DOE, Office of Science, Office of Basic Energy Sciences, Division of Chemical Sciences, Geosciences, and Biosciences. Computer time was provided by the National Energy Research Scientific Computing Center (NERSC), a U.S. DOE Office of Science User Facility operated by Lawrence Berkeley National Laboratory, and the Molecular Sciences Computing Facility (MSCF) in the Environmental Molecular Sciences Laboratory, a DOE User Facility located at the Pacific Northwest National Laboratory (PNNL). PNNL is operated by Battelle for the DOE under Contract number DE-AC05-76RL01830.

References

- (1) Burgess, B. K.; Lowe, D. J. Mechanism of Molybdenum Nitrogenase. *Chem Rev* **1996**, *96*, 2983-3012.
- (2) Hoffman, B. M.; Lukoyanov, D.; Yang, Z. Y.; Dean, D. R.; Seefeldt, L. C. Mechanism of Nitrogen Fixation by Nitrogenase: The Next Stage. *Chem Rev* **2014**, *114*, 4041-4062.
- (3) Seefeldt, L. C.; Yang, Z. Y.; Lukoyanov, D. A.; Harris, D. F.; Dean, D. R.; Raugei, S.; Hoffman, B. M. Reduction of Substrates by Nitrogenases. *Chem Rev* **2020**, *120*, 5082-5106.
- (4) Barney, B. M.; Igarashi, R. Y.; Dos Santos, P. C.; Dean, D. R.; Seefeldt, L. C. Substrate Interaction at an Iron-Sulfur Face of the FeMo-Cofactor During Nitrogenase Catalysis. *J. Biol. Chem.* **2004**, *279*, 53621-53624.
- (5) Igarashi, R. Y.; Dos Santos, P. C.; Niehaus, W. G.; Dance, I. G.; Dean, D. R.; Seefeldt, L. C. Localization of a Catalytic Intermediate Bound to the FeMo-Cofactor of Nitrogenase. *J. Biol. Chem.* **2004**, *279*, 34770-34775.
- (6) Igarashi, R. Y.; Laryukhin, M.; Dos Santos, P. C.; Lee, H. I.; Dean, D. R.; Seefeldt, L. C.; Hoffman, B. M. Trapping H- Bound to the Nitrogenase FeMo-Cofactor Active Site During H₂ Evolution: Characterization by Endor Spectroscopy. *J. Am. Chem. Soc.* **2005**, *127*, 6231-6241.
- (7) Hoeke, V.; Tociu, L.; Case, D. A.; Seefeldt, L. C.; Raugei, S.; Hoffman, B. M. High-Resolution Endor Spectroscopy Combined with Quantum Chemical Calculations Reveals the Structure of Nitrogenase Janus Intermediate E₄(4H). *J. Am. Chem. Soc.* **2019**, *141*, 11984-11996.
- (8) Lukoyanov, D.; Khadka, N.; Yang, Z. Y.; Dean, D. R.; Seefeldt, L. C.; Hoffman, B. M. Reductive Elimination of H₂ Activates Nitrogenase to Reduce the N≡N Triple Bond: Characterization of the E₄(4H) Janus Intermediate in Wild-Type Enzyme. *J. Am. Chem. Soc.* **2016**, *138*, 10674-10683.
- (9) Raugei, S.; Seefeldt, L. C.; Hoffman, B. M. Critical Computational Analysis Illuminates the Reductive-Elimination Mechanism That Activates Nitrogenase for N₂ Reduction. *PNAS* **2018**, *115*, E10521-E10530.
- (10) Barney, B. M.; Lukoyanov, D.; Igarashi, R. Y.; Laryukhin, M.; Yang, T. C.; Dean, D. R.; Hoffman, B. M.; Seefeldt, L. C. Trapping an Intermediate of Dinitrogen (N₂) Reduction on Nitrogenase. *Biochemistry* **2009**, *48*, 9094-9102.
- (11) Lukoyanov, D.; Yang, Z. Y.; Khadka, N.; Dean, D. R.; Seefeldt, L. C.; Hoffman, B. M. Identification of a Key Catalytic Intermediate Demonstrates That Nitrogenase Is Activated by the Reversible Exchange of N₂ for H₂. *J. Am. Chem. Soc.* **2015**, *137*, 3610-3615.
- (12) Lukoyanov, D.; Barney, B. M.; Dean, D. R.; Seefeldt, L. C.; Hoffman, B. M. Connecting Nitrogenase Intermediates with the Kinetic Scheme for N₂ Reduction by a Relaxation Protocol and Identification of the N₂ Binding State. *PNAS* **2007**, *104*, 1451-1455.
- (13) Christiansen, J.; Goodwin, P. J.; Lanzilotta, W. N.; Seefeldt, L. C.; Dean, D. R. Catalytic and Biophysical Properties of a Nitrogenase Apo-MoFe Protein Produced by a *Nifb*-Deletion Mutant of *Azotobacter Vinelandii*. *Biochemistry* **1998**, *37*, 12611-12623.

- (14) Georgiadis, M. M.; Komiya, H.; Chakrabarti, P.; Woo, D.; Kornuc, J. J.; Rees, D. C. Crystallographic Structure of the Nitrogenase Iron Protein from *Azotobacter Vinelandii*. *Science* **1992**, *257*, 1653-1659.
- (15) Stoll, S.; Schweiger, A. Easyspin, a Comprehensive Software Package for Spectral Simulation and Analysis in Epr. *J. Magn. Reson.* **2006**, *178*, 42-55.
- (16) Werst, M. M.; Davoust, C. E.; Hoffman, B. M. Ligand Spin Densities in Blue Copper Proteins by Q-Band Proton and Nitrogen-14 Endor Spectroscopy. *J. Am. Chem. Soc.* **2002**, *113*, 1533-1538.
- (17) Davoust, C. E.; Doan, P. E.; Hoffman, B. M. Q-Band Pulsed Electron Spin-Echo Spectrometer and Its Application to Endor and Esem. *Journal of Magnetic Resonance Series A* **1996**, *119*, 38-44.
- (18) Smith, D.; Danyal, K.; Raugei, S.; Seefeldt, L. C. Substrate Channel in Nitrogenase Revealed by a Molecular Dynamics Approach. *Biochemistry* **2014**, *53*, 2278-2285.
- (19) Becke, A. D. Density-Functional Exchange-Energy Approximation with Correct Asymptotic Behavior. *Physical Review A: Atomic, Molecular, and Optical Physics* **1988**, *38*, 3098-3100.
- (20) Perdew, J. P. Density-Functional Approximation for the Correlation Energy of the Inhomogeneous Electron Gas. *Physical Review B* **1986**, *33*, 8822-8824.
- (21) Perdew, J. P. Erratum: Density-Functional Approximation for the Correlation Energy of the Inhomogeneous Electron Gas. *Physical Review B* **1986**, *34*, 7406
- (22) Weigend, F.; Ahlrichs, R. Balanced Basis Sets of Split Valence, Triple Zeta Valence and Quadruple Zeta Valence Quality for H to Rn: Design and Assessment of Accuracy. *Phys. Chem. Chem. Phys.* **2005**, *7*, 3297-3305.
- (23) Dolg, M.; Stoll, H.; Preuss, H. Energy - Adjusted Ab Initio Pseudopotentials for the Rare Earth Elements. *J. Chem. Phys.* **1989**, *90*, 1730-1734.
- (24) Lowe, D. J.; Eady, R. R.; Thorneley, N. F. Electron-Paramagnetic-Resonance Studies on Nitrogenase of *Klebsiella Pneumoniae*. Evidence for Acetylene- and Ethylene-Nitrogenase Transient Complexes. *Biochem. J.* **1978**, *173*, 277-290.
- (25) Gurbiel, R. J.; Bolin, J., T.; Ronco, A. E.; Mortenson, L.; Hoffman, B. M. Single-Crystal Epr and Endor Study of Nitrogenase from *Clostridium Pasteurianum*. *J. Magn. Res.* **1991**, *91*, 227-240.
- (26) Spatzal, T.; Einsle, O.; Andrade, S. L. A. Analysis of the Magnetic Properties of Nitrogenase FeMo Cofactor by Single-Crystal Epr Spectroscopy. *Angewandte Chemie International Edition* **2013**, *52*, 10116-10119.
- (27) Lukoyanov, D.; Yang, Z.-Y.; Dean, D. R.; Seefeldt, L. C.; Hoffman, B. M. Is Mo Involved in Hydride Binding by the Four-Electron Reduced (E_4) Intermediate of the Nitrogenase MoFe Protein? *J. Am. Chem. Soc.* **2010**, *132*, 2526-2527.
- (28) True, A. E.; Mclean, P.; Nelson, M. J.; Ormejohnson, W. H.; Hoffman, B. M. Comparison of Wild-Type and Nifv Mutant Molybdenum-Iron Proteins of Nitrogenase from *Klebsiella-Pneumoniae* by Endor Spectroscopy. *J. Am. Chem. Soc.* **1990**, *112*, 651-657.
- (29) Lukoyanov, D.; Yang, Z. Y.; Duval, S.; Danyal, K.; Dean, D. R.; Seefeldt, L. C.; Hoffman, B. M. A Confirmation of the Quench-Cryoannealing Relaxation Protocol for Identifying Reduction States of Freeze-Trapped Nitrogenase Intermediates. *Inorg. Chem.* **2014**, *53*, 3688-3693.
- (30) Danyal, K.; Shaw, S.; Page, T. R.; Duval, S.; Horitani, M.; Marts, A. R.; Lukoyanov, D.; Dean, D. R.; Raugei, S.; Hoffman, B. M.; Seefeldt, L. C.; Antony, E. Negative Cooperativity in the Nitrogenase Fe Protein Electron Delivery Cycle. *PNAS* **2016**, *113*, E5783-E5791.
- (31) Thorneley, R. N. F.; Lowe, D. J. Kinetics and Mechanism of the Nitrogenase Enzyme System. *Metal Ions in Biology* **1985**, *7*, 221-284.
- (32) Fisher, K.; Lowe, D. J.; Thorneley, R. N. F. *Klebsiella Pneumoniae* Nitrogenase. The Pre-Steady-State Kinetics of MoFe-Protein Reduction and Hydrogen Evolution under Conditions of Limiting Electron Flux Show That the Rates of Association with the Fe-Protein and Electron Transfer Are Independent of the Oxidation Level of the MoFe-Protein. *Biochemical Journal* **1991**, *279*, 81-85.
- (33) Lukoyanov, D. A.; Khadka, N.; Yang, Z. Y.; Dean, D. R.; Seefeldt, L. C.; Hoffman, B. M. Hydride Conformers of the Nitrogenase FeMo-Cofactor Two-Electron Reduced State $E_2(2H)$, Assigned

Using Cryogenic Intra Electron Paramagnetic Resonance Cavity Photolysis. *Inorg. Chem.* **2018**, *57*, 6847-6852.

(34) Lukoyanov, D. A.; Yang, Z. Y.; Dean, D. R.; Seefeldt, L. C.; Raugei, S.; Hoffman, B. M. Electron Redistribution within the Nitrogenase Active Site FeMo-Cofactor During Reductive Elimination of H₂ to Achieve N≡N Triple-Bond Activation. *J. Am. Chem. Soc.* **2020**, *142*, 21679-21690.

(35) We note an alternative, more extensive modification has been considered, in which the H-S2B sulfhydryl actually is lost during the catalytic cycle and regained by its end.

(36) Einsle, O.; Rees, D. C. Structural Enzymology of Nitrogenase Enzymes. *Chem. Rev.* **2020**, *120*, 4969-5004.

(37) Thorhallsson, A. T.; Bjornsson, R. The E₂ State of FeMoco: Hydride Formation Versus Fe Reduction and a Mechanism for H₂ Evolution. *Chemistry* **2021**, *27*, 16788-16800.

(38) Cao, L.; Ryde, U. What Is the Structure of the E₄ Intermediate in Nitrogenase? *J Chem Theory Comput* **2020**, *16*, 1936-1952.

(39) Lukoyanov, D.; Khadka, N.; Yang, Z. Y.; Dean, D. R.; Seefeldt, L. C.; Hoffman, B. M. Reversible Photoinduced Reductive Elimination of H₂ from the Nitrogenase Dihydride State, the E₄(4H) Janus Intermediate. *J. Am. Chem. Soc.* **2016**, *138*, 1320-1327.

(40) Lukoyanov, D.; Khadka, N.; Dean, D. R.; Raugei, S.; Seefeldt, L. C.; Hoffman, B. M. Photoinduced Reductive Elimination of H₂ from the Nitrogenase Dihydride (Janus) State Involves a FeMo-Cofactor-H₂ Intermediate. *Inorg. Chem.* **2017**, *56*, 2233-2240.